Soft Matter

PAPER

View Article Online
View Journal

Cite this: DOI: 10.1039/d5sm00979k

Dynamic droplet behavior for analyte localization on phase change liquid infused surfaces

Gregory Parisi, Allison Elliott and Samantha A. McBride *

Phase-change liquid infused surfaces (PC-LIS) can enable responsive and adaptable interfacial control due to their tunable physical properties, including wetting behavior. These materials leverage the phase transition of oils/waxes infused within a micro- or nano-texture to dynamically alter their interfacial properties. Using thermal control, PC-LIS are able to dynamically switch between solid states in which droplet contact lines are more easily pinned and liquid states where droplet contact lines are mobile. This enables them to harness the slippery, anti-fouling behavior of LIS while also improving material durability to variable conditions such as abrasion or shearing flows, which can deplete lubricant from traditional, static LIS. Here, we demonstrate how the surface morphology and phase state of PC-LIS can be used to control dynamics of drops evaporating on the surfaces as well as the associated microparticle deposition outcomes. We report on how phase-switching controls contact angle hysteresis, sliding angle, and evaporation mode of drops to enable precise control over droplet mobility and deposition footprint. By using these materials to substantially reduce deposit footprint, we can enable new, simple methods for analyte localization for environmental sensing. This is especially important for dilute physical contaminants such as micro- and nano-plastic fragments. Using model plastic microparticles as well as real microplastics from plastic bottled drinking water, we demonstrate that PC-LIS can successfully concentrate analytes into a small, localized region for analysis by evaporating drops on surfaces in the liquid configuration. Following analyte localization, the materials can be reverted back to the solid configuration for detection using other techniques.

Received 26th September 2025,
Accepted 11th January 2026

DOI: 10.1039/d5sm00979k

rsc.li/soft-matter-journal

Introduction

Liquid infused surfaces (LIS) are a class of engineered interfaces that exhibit exceptional liquid repellency and droplet mobility.[1] Inspired by the Nepenthes pitcher plant, LIS operate by infusing a lubricating liquid into a micro- or nano-textured solid matrix.[2] This creates a smooth, defect-free interface where working fluids in contact with the surface experience minimal contact angle hysteresis and negligible pinning.[3,4] As a result, LIS have found broad applications in anti-fouling,[5–8] condensation heat transfer,[9–11] nanogenerators,[12] anti-icing surfaces,[13] and droplet manipulation.[14]

Despite their versatility, traditional LIS face some limitations that constrain their practical deployment.[15] Once infused, their surface properties remain largely fixed, lacking dynamic responsiveness to environmental stimuli. Traditional LIS also have limited mechanical durability due to lubricant depletion under shearing flows and susceptibility to damage under abrasion.[16–18] Thus, the ability to reversibly solidify the imbued lubricant can improve durability by maintaining the surface in the solid phase when it is subjected to abrasion or shearing forces, and only liquifying the lubricant to recover slippery properties as needed for a target application.[19,20]

Phase change LIS (PC-LIS) address these challenges by enabling switchable wettability through thermal modulation of the infused oil's phase for alternation between a rigid, textured state and a lubricated, low-friction interface.[21] When heated above their melting point, infused oils liquefy to restore the mobility and low hysteresis characteristic of classical LIS. Switchable wettability has been applied for numerous applications,[22,23] including thermal management,[24–26] analyte sensing,[27] optics,[28] oil–water separation,[29] and fog harvesting.[30] Here, we are interested in two key advantages enabled by PC-LIS. First, the ability to reversibly solidify the lubricant improves durability by maintaining the lubricant in a solid, damage-resistant state between activation cycles.[31] Second, thermal control over wetting behavior enables dynamic manipulation for applications requiring precise control over droplet motion, adhesion, and evaporation.[32–34]

Recent work has demonstrated the durability benefits of PC-LIS across multiple applications. Work by Jiang and colleagues demonstrated enhanced durability with a paraffin wax-infused carbon steel surface actuated using NIR irradiation for anti-fouling and anticorrosion applications.[35] Similarly, Ye *et al.*

Mechanical Engineering and Applied Mechanics, University of Pennsylvania, 3451 Walnut Street, Philadelphia, PA 19104, USA. E-mail: sammcb@seas.upenn.edu

created a PC-LIS using anodized aluminum oxide and paraffin wax for passive, sustainable, and durable anti-scaling.[36] PC-LIS have also been designed for improving anti-frosting and condensation applications,[37] and for self-healing by melting and re-solidifcation of the wax.[38,39]

Beyond durability, PC-LIS can enable precise control over droplet evaporation dynamics, which have important applications for analyte localization and sensing.[40] Droplet evaporation typically proceeeds in one of two distinct modes: constant contact angle (CCA), where the droplet radius recedes with a fixed angle, and constant contact radius (CCR), where the contact line remains pinned while the contact angle decreases.[41,42] The substrate properties that control evaporation mode are critical for also controlling heat and mass transfer rates, droplet lifetime, and the final deposition pattern of solutes or particulates.[43,44] Traditional LIS can suppress crystalline ring deposition by preventing contact line pinning through the presence of a lubricating oil to create highly condensed, localized deposits.[44,45] This ability is valuable for applications in sensing and diagnostics where spatial localization enhanced signal sensitivity and resolution.[46–48] Prior work has applied LIS for extreme localization of gold nanoparticles alongside target analytes for surface-enhanced Raman Spectroscopy, and demonstrated that the platform enables detection down to subfemtomolar concentrations.[48] PC-LIS extend this functionality by enabling thermal control between pinning and mobile states, allowing dynamic control over where and how analytes.

Dynamic control over analyte deposition can be particularly powerful for detecting dilute environmental contaminants such as microplastics, which can be challenging to detect using traditional techniques.[49,50] Many microplastic detection methods rely on bulk filtration followed by microscopy and spectroscopy. These techniques are time-intensive, require specialized facilities, and often expensive.[51] Surface-enabled droplet evaporation platforms are a potential solution, as they can concentrate and isolate particulates for microplastic detection and remediation.[52–55] PC-LIS can enhance this approach by enabling droplet manipulation and localization in the liquid state followed by solidification for compatibility with analytical techniques that are incompatible with liquid substrates.

Here, we explore how the properties of PC-LIS can be altered to enable both enhanced durability as well as precise control over droplet evaporation dynamics using beeswax, coconut oil, and paraffin waxes as the infused phase. While many properties of PC-LIS have been explored by past work, we report on the evaporation dynamics of drops on these materials across lubricant states for the first time. We explore how the oil phase state (liquid or solid) and surface roughness govern drop evaporation mode transitions between CCR and CCA, and quantify the impact of the phase transitions on contact angle, contact angle hysteresis, and sliding angle. Using optical profilometry and scanning electron microscopy (SEM), we characterize the surface roughness and morphology of the oils in different states. Finally, we demonstrate a new functional application of PC-LIS in analyte sensing using both model and real microplastics within droplets to illustrate how thermal switching enables controlled deposition. We also assess the durability of PC-LIS under sonication and abrasion to evaluate their reusability and stability under mechanical stress. Our results reveal that PC-LIS can offer a tunable and durable platform for evaporation control and environmental sensing.

Methods

Substrate fabrication

Silicon wafers (P/B, WaferPro) were etched using deep-reactive ion etch (SPTS Si DRIE, Rapier) to create microscale surface roughness, which is typically referred to as nanograss or black silicon.[56,57] The surface was modified using trichloro (1*H*,1*H*,2*H*,2*H*-perfluorooctyl) silane (97%, TCI) by vapor deposition for 6 hours following plasma clean surface activation. The resulting surfaces were analyzed by SEM (TFS Quanta 600 FEG ESEM, Thermo Fisher Scientific) to confirm surface texturing (Fig. 1a). Samples were then diced into 1.5 × 1.5 cm^2 pieces using a dicing saw (7100 Dicing Saw, Advanced Dicing Technologies) prior to use for PC-LIS.

PC-LIS preparation

PC-LIS were prepared by infusing textured silicon surfaces with one of four different types of materials - silicone oil (non-phase change control), coconut oil, paraffin wax, or beeswax. A variety of infused oils were selected to capture differences in physical and chemical properties that directly influence wettability and evaporation. The naturally-derived oils (coconut oil and beeswax) were selected to align with principles of green and sustainable chemistry. Prior to infusion, the static water contact angle of each surface was measured to confirm hydrophobicity, and both apparent surface area and initial mass were recorded. Here, apparent surface area refers to the projected sample area measured from top-down optical images in ImageJ, which will differ somewhat from overall surface area when the nanotexture is considered. Lubricant was infused into the nanotextured surfaces by heating the nanograss coupons to slightly above the lubricant's melting point (Fig. S5) followed by spreading of liquid oil across the surface. Following this oil addition step, the sample was reweighed to calculate the total mass of added oil.

Oil-coated nanograss samples were transferred to a vacuum drying oven (Across International Eco Drying Oven) maintained at a temperature of at least 10 °C above each oil's melting point. This temperature was set at 36 °C for coconut oil, 75 °C for beeswax, and 78 °C for paraffin wax. Since silicone oil does not experience phase change, the temperature of the vacuum drying oven was arbitrary for these samples. The oven was then brought to a full vacuum for 15 minutes, after which each sample was vertically annealed on one side for 5 minutes. Samples were then placed face-down inside the vacuum oven with the oil infused surface in contact with the oven plate and held under vacuum for an additional 15 minutes, following procedures established by others for reducing excess oil.[58] Finally, samples were vertically annealed on all four sides, for

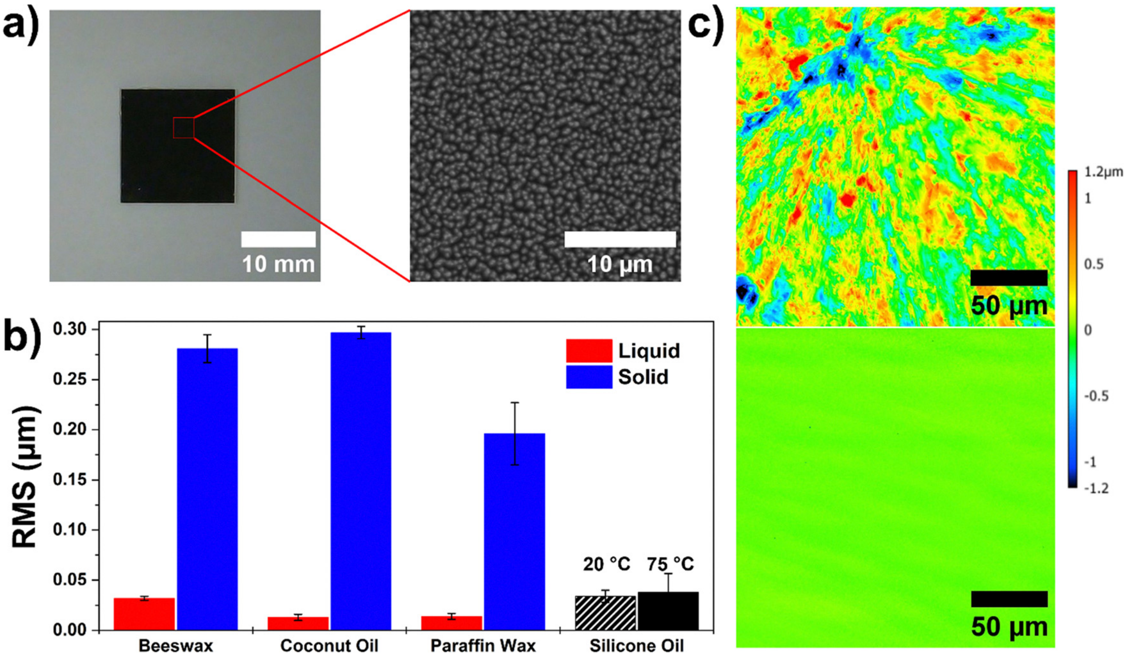

Fig. 1 Surface morphology and roughness characterization of PC-LIS samples. (a) Photograph and SEM image of etched silicon wafer used as the porous substrate for lubricant infusion. (b) RMS roughness of each oil in the liquid and solid state. (c) 3D optical profilometry scans of coconut oil in solid (top) and liquid states (bottom).

5 minutes per side, with the bottom of the sample blotted in between steps to remove excess oil. At the end of this process, the final mass of each sample was recorded to calculate oil loss during the infusion process.

Additional samples prepared using excess oil methods (*i.e.*, fewer annealing steps) were also tested for selected experiments with fabrication methods described in Text S1. We determined that the above procedure minimized excess lubricant interference during evaporation, ensuring more consistent droplet-substrate interaction, in alignment with prior findings.[58]

Wettability characterization

Wetting properties including static water contact angle (WCA), sliding angle (SA), and contact angle hysteresis (CAH) were characterized for all samples across their solid, mush, and liquid phases using a Krüss contact angle goniometer. The experimental setup consisted of a small heater (Watlow, Ultramic) clamped to the goniometer stage and connected to a tunable DC power supply for precise temperature control. The solid phase temperatures were set to either 20 or 25 °C and the liquid phase temperatures were all set to 75 °C. Thermal paste (AOS, 340 WC) was applied to the surface of the heater to improve thermal conduction between the heater and the PC-LIS.

Measurements were performed in triplicate at three different locations on the sample to account for any variations in surface texture. Temperature settings were adjusted according to the phase transition temperatures of each oil, with exact values provided in Table S1.

For each experiment, a 5 μL deionized water droplet was dispensed onto the sample surface. Static water contact angles were recorded using the goniometer. To measure droplet sliding angle and contact angle hysteresis, the goniometer stage was tilted at a rate of 1° per second. Video analysis was used to determine the moment at which the droplet depins from the surface and for determination of the advancing angle, receding angle, and sliding angle. The sliding angle was calculated by multiplying the depinning time by the tilt rate. Contact angle hysteresis was calculated by taking the difference between the advancing and receding angles.

Evaporation testing

Evaporation behavior was evaluated to assess PC-LIS performance under dynamic thermal conditions. These measurements used the same experimental setup as the wettability characterization procedures. A 5 μL deionized water droplet was deposited onto the surface of each sample and the droplet profile was recorded until evaporation was complete. Evaporation experiments were conducted at different temperatures to capture drop dynamics on both solid and liquid phases. Measurements for droplet water contact angle, radius, and volume were automatically extracted at periodic intervals. Room temperature in the controlled lab environment was monitored throughout all experiments and remained consistent at 20 C ± 1 °C. Humidity was similarly recorded and remained at 49 ± 9%. Full details of environmental conditions are available in Table S2.

After the droplet had fully evaporated, total evaporation time, evaporation rate, and evaporation flux were extracted from videos. The evaporation rate ($\dot{V}$) in between measurements was calculated as $\dot{V} = \Delta V/\Delta t$, where ΔV is the change in volume and Δt is the elapsed time.

Surface roughness and profilometry

An optical profilometer (Keyence Profilometer) was used to assess RMS surface roughness of each oil in both liquid and solid states. The optical profilometer was also used for 3D height mapping and surface topography.

Durability testing

Samples were subjected to water sonication (Emerson Branson, MH Series) and abrasion with a weighted Kimwipe drag test. For the water sonication, samples were placed in a 50 mL beaker of water and subjected to sonication for a specific time duration (0, 5, 10, and 15 min).[59] The abrasion test was performed by placing a 50 g weight on top of the sample which was face down on a Kimwipe. It was then dragged across the Kimwipe for a specific distance (0, 50, 100, and 150 cm).[60] Post-treatment wetting was evaluated using the drop shape analyzer.

Microplastic sensing

Particle-laden droplets (3 μL) were evaporated on PC-LIS surfaces as a model for microplastic or other particulate analytes. Fluorescence microscopy (Zeiss, Axio Zoom V16) was used to quantify final deposition area. The model microplastic solution was prepared by adding 0.01% by volume of 1 μm microspheres (Degradex PLGA, Phosphorex) to DI water.[61] This concentration was selected as a balance of a strong signal while also being reasonably dilute. Real microplastics were also prepared from commercially available plastic (PET) bottled water (Nestle Pure Life). Water from the plastic bottles were poured into a clean glass container. A mixture of acetone with 1 mg mL^{-1} nile red was then added to the water for an overall volumetric concentration of 3 : 1 water to acetone/nile red.[62] The solution was heated at 70 °C for 30 minutes to fluorescently stain the microplastics. Stained microplastics were then used in drop evaporation experiments at the original concentration of the bottled water. Using particle counting methods, we estimate this concentration to be roughly 6000 particles per liter (limit of detection $\sim$1 μm), which is in line with published data for the same brand which estimated 40–10 000 counts of particles per liter.[63] Because real microplastics exhibit massive size distributions, it is challenging to translate this particle count into an estimated volume concentration.

Results

PC-LIS surface morphology & stability

Wettability describes how a liquid interacts with a solid surface and is typically characterized by the contact angle as a measure of how readily a droplet spreads over a given surface.[64] Low contact angles indicate strong adhesion and high wettability, while high angles generally suggest weak interaction and greater mobility.[65] Wetting is governed by the balance of interfacial tensions, as described by Young's equation.[66] Surface roughness modifies wetting behavior and can either increase or decrease droplet pinning and mobility depending on texture and chemistry.[67,68] In LIS, roughness at the nano/micro-scale is used to retain lubricant retention *via* capillary forces. LIS exhibit strongly tunable evaporation-driven deposition behavior, with lubricant thickness and viscosity significantly influencing droplet mobility and resulting particle patterns.[69] When the liquid is infused within the texture, the surface becomes smooth and low-friction with minimized contact angle hysteresis.[70]

PC-LIS function in much the same way as LIS, except that the lubricant can reversibly solidify or liquify. This phase-switching capability introduces unique thermodynamic considerations. In the liquid phase, PC-LIS exhibit the same characteristic low-friction, slippery behavior of traditional LIS with drops maintained in a mobile state through a thin lubricating film. In the solid state, many PC-LIS allow for droplet pinning in a high-adhesion Wenzel state on the rough, solidified wax surface;[20] although recent work on precisely tuning the wax loading and thickness has allowed for maintainance of low-adhesion even in the solid phase.[85] The transition between states is driven by phase change enthalpy of the infused material. Organic phase change materials such as the paraffin waxes and naturally occurring waxes typically have latent heats ranging from 150–250 J g^{-1}.[71] In between the solid and liquid phases is the so-called "mush" phase, where the wax exists as a mixture of solid and liquid phases. Prior work on the mush phase has found a complex relationship between adhesion and phase-state of the imbued fluid.[72]

Surface morphology plays a critical role in determining droplet–surface interactions, including contact line pinning, lubricant retention, and the transition between Wenzel and Cassie–Baxter wetting regimes.[73] Fig. 1a shows the nanostructure of the etched superhydrophobic silicon wafer used to fabricate the PC-LIS. The infused oils significantly modified the surface topography depending on their phase state. In the solid state, phase change oils formed crystalline structures that increased surface roughness, resulting in elevated RMS values of 0.281 μm for beeswax, 0.297 μm for coconut oil, and 0.196 μm for paraffin wax (Fig. 1b). In contrast, when in the liquid phase, the same oil produced a smooth, low-roughness interface (RMS < 0.05 μm) consistent with other liquid-infused surfaces, with RMS values of 0.032 μm for beeswax, 0.013 μm for coconut oil, and 0.014 μm for paraffin wax. Fig. 1c shows profilometer images of coconut oil in its solid and liquid states. Images for paraffin wax and beeswax, which exhibit similar phase-dependent topographical changes, are shown in Fig. S1. Silicone oil, which does not undergo a phase change and lacks switchable wettability, was used as a control in all experiments and exhibited consistent surface morphology across temperatures (Fig. 1b).

In these experiments, some of the tested waxes exhibited an increased contact angle in the solid, waxy state *vs.* in the liquid, oil state, reflecting a change in roughness (as famously described by the Wenzel equation[74]) (Fig. 2a). For example, drops on paraffin wax exhibited a rise in water contact angle from 104° in the liquid phase to 112° in the solid phase, suggesting increased roughness ($r \sim 1.54$) in the solid phase and therefore an increase in the measured contact angle.

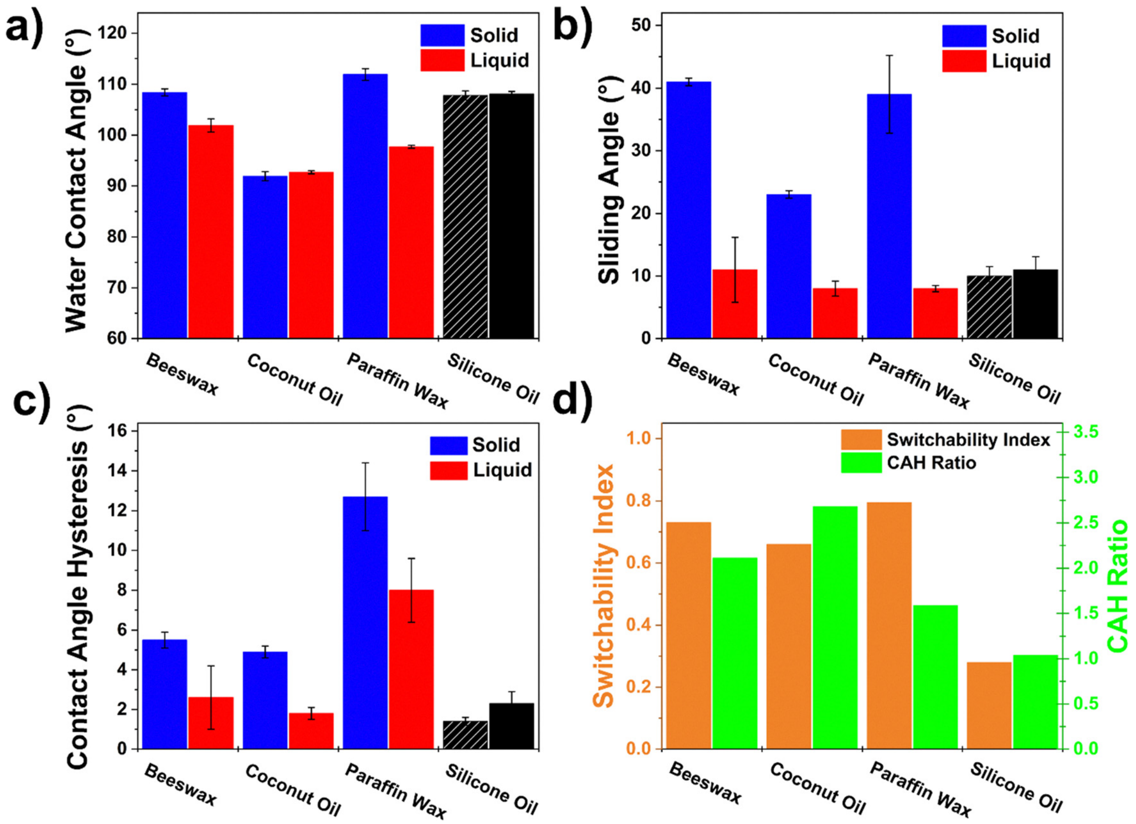

Fig. 2 Wettability of PC-LIS. (a) Static water contact angle (WCA), (b) sliding angle, and (c) contact angle hysteresis (CAH) measurements comparing the solid and liquid phases of each oil, and at two different temperatures for silicone oil (20 °C and 75 °C). (d) Quantification of the switchability index and CAH ratio. For the control, silicone oil, the striped black bar indicates 20 °C and the solid black bar indicates 75 °C.

While the Wenzel equation can be used for describing the roughness of the PC-LIS and contact angle of a drop of water wetting the surface while the wax is in the solid state, the Cassie–Baxter equation can be applied to describe the impregnation of the oil into the microtexture and its stability while in the liquid state.[75] Wetting ridge area was also measured for each PC-LIS sample to evaluate how oil type and layer thickness affect interfacial deformation at the droplet boundary. For this measurement, wetting ridge area was calculated from side-profile images taken during the evaporation experiments. Among the four oils tested, silicone oil produced the largest wetting ridge, followed by beeswax and paraffin wax, while coconut oil yielded the smallest ridge.

All surface morphology data for PC-LIS made using both the optimized and excess oil fabrication methods are included in Fig. S3. The material parameters used here were selected to study droplet evaporation response to surface phase rather than to independently probe their influence on evaporation, and these factors may be systematically varied in future work to quantify their individual contributions.

Phase-dependent wettability and sliding behavior

Fig. 2a–c shows the static water contact angle (WCA), sliding angle (SA), and contact angle hysteresis (CAH) across all tested oils and phases. In the solid phase, the PC-LIS exhibit reasonably low CAH ($<15°$) and sliding angles between 25° and 45°, indicating moderate pinning. As the oils transition to the liquid phase, CAH values decrease for all phase change oils. Similarly, SA drops significantly for coconut oil, beeswax, and paraffin wax, confirming restoration of the LIS effect at elevated temperatures. Since the silicone oil is not a phase change liquid, the data for silicone oil was taken at a low and high temperature to control for temperature effects. The 3° difference in sliding angle measured for silicone oil between the 20 °C and 75 °C conditions lies within the standard deviation of the measurement and is not likely to be statistically significant.

The observed wetting behavior across phases is consistent with the combined influence of surface roughness and interfacial tension.[76] The transition from solid to liquid phase reduces solid–liquid interfacial friction and pinning forces. This behavior is quantitatively characterized by the switchability index (SI), defined here as:

$$\mathrm{SI} = \frac{\mathrm{SA_s} - \mathrm{SA_l}}{\mathrm{SA_l}}$$

where SA is the sliding angle in the solid ($\mathrm{SA_s}$) or liquid ($\mathrm{SA_l}$) phase. Higher SI values indicate a greater degree of tunability and reversibility of the wetting state between the phases (Fig. 2d). Coconut oil and beeswax demonstrated a moderate SI (0.66 and 0.73 respectively), while paraffin wax showed the most substantial switching (0.79) of all tested materials. The SI of silicone oil should be nominally zero, but had a discrete value here ($\sim$0.25) due to the minor variation in sliding angles at different temperatures despite not switching phases.

For applications in analyte manipulation, low substrate CAH is desirable as it allows for analytes within a drop to be effectively localized. Predictably, all phase-change LIS exhibited a significantly lower CAH while in the liquid phase than in the solid (Fig. 2c), indicating greater droplet mobility. The degree of difference between the solid and liquid phase CAH can be quantified using the CAH ratio, defined as

$$\text{CAH ratio} = \frac{\text{CAH}_\text{s} - \text{CAH}_\text{l}}{\text{CAH}_\text{l}}$$

Trends between the CAH and SI were more or less consistent across the tested materials, with the exception of paraffin wax which exhibited the highest SI but lowest CAH ratio. In general, low CAH is typically associated with a correspondingly low SA. However, this relationship is not guaranteed and can be influenced by other factors such as the specific texture, directionality of the roughness,[77] and gravitational force on the probe droplet for SA measurements. The idea that specific texture and directionality may have influenced the relationship between SA and CAH here is supported by images of solid-state wax materials (Fig. S1), where there are significant differences in the texture morphology between the beeswax, paraffin wax, and coconut oil solid PC-LIS materials.

To better understand the physical origin of the phase-dependent wetting behavior, we summarize the viscosity of each lubricant in both solid and liquid states and compare it to the corresponding mobility metric, CAH/η. Table 1 shows how phase dependent viscosity governs interfacial resistance and controls the observed changes in CAH, sliding angle, and droplet mobility across the different lubricants.[78] In the solid state, all three oils exhibit extremely high effective viscosities on the order of 10^6 to 10^7 mPa s, which dramatically increases resistance to interfacial shear and suppresses motion at the wetting ridge.[79] This large viscous dissipation results in strong contact line pinning, reflected in the low CAH/η ratios. Coconut oil exhibits the lowest solid-phase viscosity amongst the three, consistent with its slightly lower solid-state CAH and sliding angle. Paraffin wax and beeswax, which form more rigid crystalline networks upon cooling, both have higher viscosities compared to coconut oil. Upon melting, the lubricant decreases in viscosity, which reduces its resistance and restores LIS-like droplet mobility. Because the sliding angle reflects the force required to overcome contact line pinning, it increases with CAH, as larger hysteresis corresponds to stronger resistance to droplet motion.

Table 1 Summary of lubricant viscosities corresponding to CAH mobility ratios

Lubricant	Phase	Viscosity [mPa s] (η)	CAH/η
Coconut oil	Solid[80]	$\sim 10^6$	5×10^{-6}
	Liquid[81]	35	0.06
Paraffin wax[82]	Solid	$\sim 10^7$	1×10^{-6}
	Liquid	7	1.1
Beeswax	Solid[83]	$\sim 10^7$	7×10^{-7}
	Liquid[84]	25	0.2

The mush phase, which is defined as the semi-solid, semi-liquid transitional state near the melting point of the infused oil,[85] exhibited intermediate behavior in all wetting characteristics, as shown in Fig. S4. This phase arises due to incomplete melting or recrystallization, resulting in heterogeneous surface properties and unstable wetting behavior. While it may offer limited tunability, the mush phase is generally undesirable for most applications due to its inconsistent surface performance and lack of reproducibility.

Correlation between wetting and evaporation modes

The relationship between wetting states and drop evaporation modes has been widely studied, with prior work showing that surfaces with low contact angle hysteresis and mobile contact lines typically favor the constant contact angle (CCA) mode, while rough or pinned surfaces promote constant contact radius (CCR) evaporation. These different evaporation behaviors, driven by variations in substrate surface energy, directly affect how particles deposit or how patterns form from saline drop evaporation.[7,86–88] For example, Guan *et al.*[41] demonstrated that LIS and other smooth, low-friction surfaces support CCA evaporation due to enhanced contact line mobility. Armstrong *et al.*[89] showed that electrowetting coupled with a slippery infused surface can control the evaporation dynamics on command.

Droplet evaporation experiments were conducted on all PC-LIS as well as the silicone oil LIS at temperatures of 75 °C (where all 3 waxes are firmly in the liquid phase) and 20 °C to compare liquid-state and solid-state evaporation dynamics (Fig. 3). The propagation of uncertainty was calculated for evaporation tests and is explained in Text S2. In the liquid phase, drops on all oils showed evaporation behavior consistent with a constant contact angle (CCA) mode, as indicated by a steady decrease in droplet radius and a relatively smooth decline in contact angle (Fig. 3b/d). This behavior reflects a low-pinning interface where the contact line recedes continuously, allowing for rapid evaporation and compact deposition. The reduced contact angle hysteresis in the liquid state could assist in maintaining any particles within the drop near the center of the droplet during evaporation. In contrast, drops on the solid-phase PC-LIS exhibited constant contact radius (CCR) mode in the very early stages of evaporation, characterized by a relatively stable droplet base radius and a gradual decline in contact angle (Fig. 3a/c). This CCR stage persisted for approximately 500–1000 seconds for the three wax materials (Fig. 3c), suggesting that contact line pinning dominates initially. Contact line pinning is likely due to increased surface roughness and rigidity of the solidified oils compared to their liquid phase, where drop contact radius starts to drop immediately (Fig. 3d). As evaporation progresses, drops on the solid phase PC-LIS eventually depin and the contact line recedes as droplet volume diminishes. This leads to a partial transition to mixed-mode evaporation, which is a classic behavior for evaporation that initiates in CCR mode.[90] This combination of early CCR and later-stage

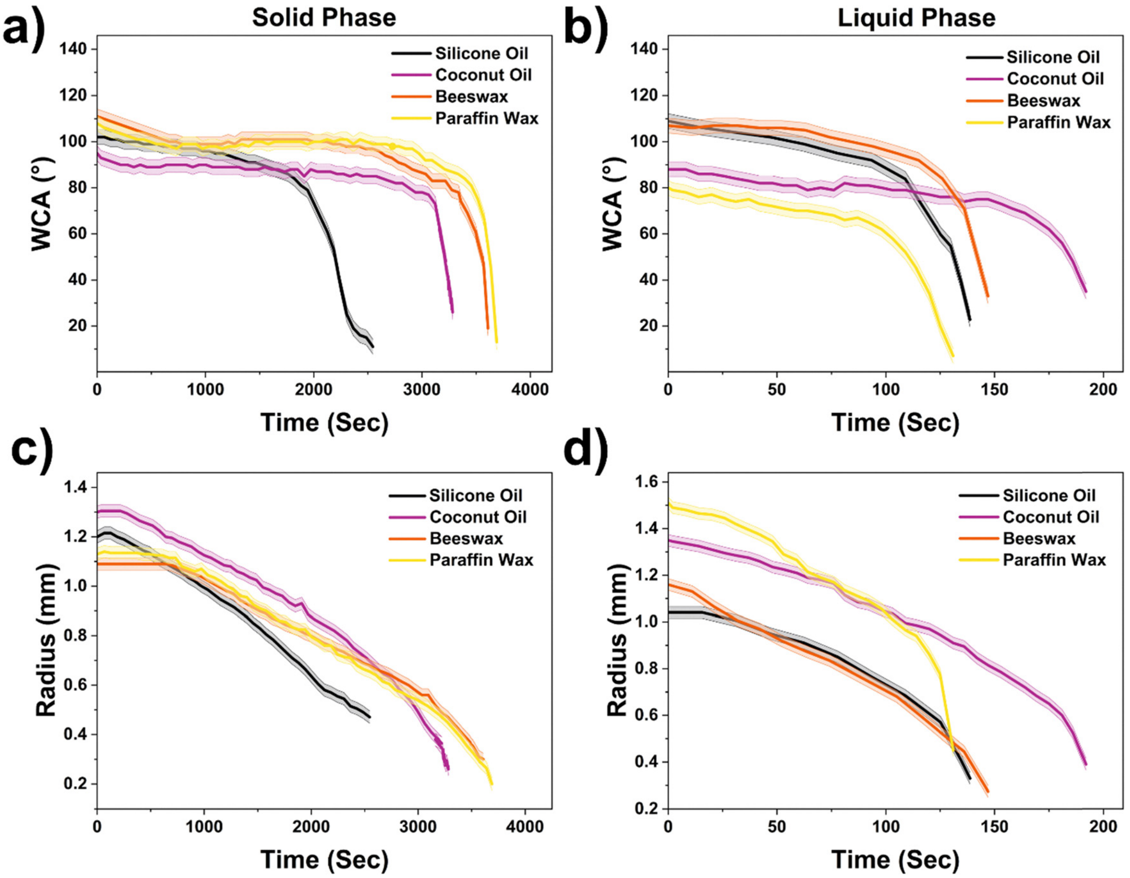

Fig. 3 Evaporation dynamics on PC-LIS surfaces in solid and liquid states. (a and b) Time-resolved water contact angle (WCA) and (c and d) base radius evolution for droplets evaporating on solid-phase (left) and liquid-phase (right) PC-LIS. Parts a, c show evaporation dynamics at 20 °C where all waxes are in the solid phase, while parts b, d show show dynamics at 75 °C where all waxes are in the liquid phase.

movement contributes to longer evaporation times and broader deposition areas compared to CCA evaporation dynamics.

We estimated the characteristic dimensionless numbers governing droplet shape, interfacial motion, and particle transport during evaporation to identify the dominant forces controlling CCR and CCA evaporation modes. For a 5 μL water droplet with a radius (R) of ∼1.1 mm, the Bond number ($\mathrm{Bo} = \rho g R^2/\gamma$), where ρ is the density of the fluid, g is the gravitational constant, and γ is the surface tension of the fluid, is approximately 0.1 to 0.2, confirming that droplet shape on all surfaces is capillary dominated.[91] Additionally, the Capillary number ($\mathrm{Ca} = \eta \bar{U}/\gamma$), where η is the viscosity of the fluid and $\bar{U}$ is the average radial velocity induced by droplet evaporation, remains very small under the estimated contact line velocities for both liquid and solid phases, indicating the vapor concentration field is quasi-steady.[92] Since $\mathrm{Bo} < 1$ and $\mathrm{Ca} \ll 1$, CCR and CCA behavior must arise from contact line pinning instead of gravity or viscous forces.

For evaporation of drops on the liquid phase materials at 75 °C (Fig. 3b/d), drops on the paraffin wax exhibited the highest evaporation rate, followed by silicone oil and beeswax (Fig. 4b). Drops on coconut oil required the longest time for full evaporation. The difference in evaporation rates on the liquid surfaces can be partially explained by the differences in initial WCA, where smaller WCAs lead to larger initial contact radius and therefore more heat transfer. This can explain why drops on paraffin wax evaporated the fastest due to the initially larger radius (Fig. 3d) as well as the trends for drops on beeswax and silicone oil. However, the evaporation rate of drops on the coconut oil PC-LIS deviates from this trend, exhibiting the longest evaporation time despite having a relatively large initial radius of approximately 1.4 mm. Thermal conductivity for all four oils is approximately the same with values ranging from 0.15 to 0.25 W m^{-1} K^{-1}. One potential explanation for the longer drop evaporation timescale on the coconut oil surfaces may be due to the minimal contact angle hysteresis on this surface, with the drop evaporating in nearly constant contact angle mode for a longer period of time compared to the other materials.

In the solid phase, all tests were performed at room temperature 20 °C ± 1 °C (Fig. 3a/c). When solidified, oil crystallinity and surface structure will dominate drop pinning and evaporation behavior. Drops on silicone oil exhibited the fastest evaporation rate, followed by drops on coconut oil and then by drops on the beeswax and paraffin wax (Fig. 4a). This trend likely reflects how the solid state affects contact line pinning. Paraffin wax and beeswax both form crystalline or semicrystalline rough waxy layers which lead to initial pinning for

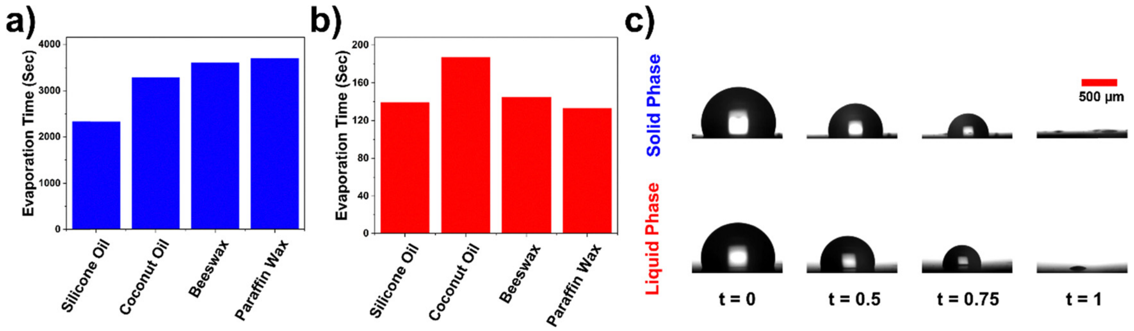

Fig. 4 Evaporation rates for drops on each material in the (a) solid (20 °C) and (b) liquid states (75 °C) (c) side-profile images of beeswax during evaporation.

~1000 s (CCR mode) at the onset of drop evaporation before transitioning to CCA mode, and then finally mixed mode towards the end. Although drops on coconut oil spent less time in CCR mode (~500 s) at the onset of evaporation due to lower CAH on the solid, its initially higher WCA led to more contact area and therefore slightly faster evaporation compared to drops on the beeswax and paraffin wax. Silicone oil, which does not undergo a phase change and remained liquid even at the 20 °C condition, maintained mobility for most of its evaporative process. However, it evaporated faster compared to the three solid waxes. In general, drop evaporation should be slower on interfaces that maintain mobility and allow for CCA evaporation compared to interfaces where drops pin in place and therefore have more contact area between the drop and heated substrate.

Side-profile snapshots of droplets on beeswax surfaces during evaporation show differences between liquid-state evaporation at 75 °C and solid state evaporation at 20 °C at different timepoints normalized to the total evaporation time (Fig. 4c). The liquid phase profile shows steady retreat that is not quite CCA but is also not fully pinned, while the solid phase maintains a broader base with a more rapid decrease in curvature.

Applications for durable microplastic sensing

After quantifying the droplet evaporation dynamics on PC-LIS in both solid and liquid states, we demonstrate that these surfaces can be used for spatial control over evaporative deposition of model microplastics using fluorescent polystyrene spheres. When droplets evaporate on liquid-phase PC-LIS, the low hysteresis and mobile interface induce recirculating Marangoni flows that concentrate analytes at the center of the droplet footprint, resulting in a small, highly localized fluorescent spot[93] as shown in Fig. 5a. Further investigation of internal Marangoni and capillary flow fields could provide additional insight into how these mechanisms interact with contact line mobility. In contrast, the contact line on

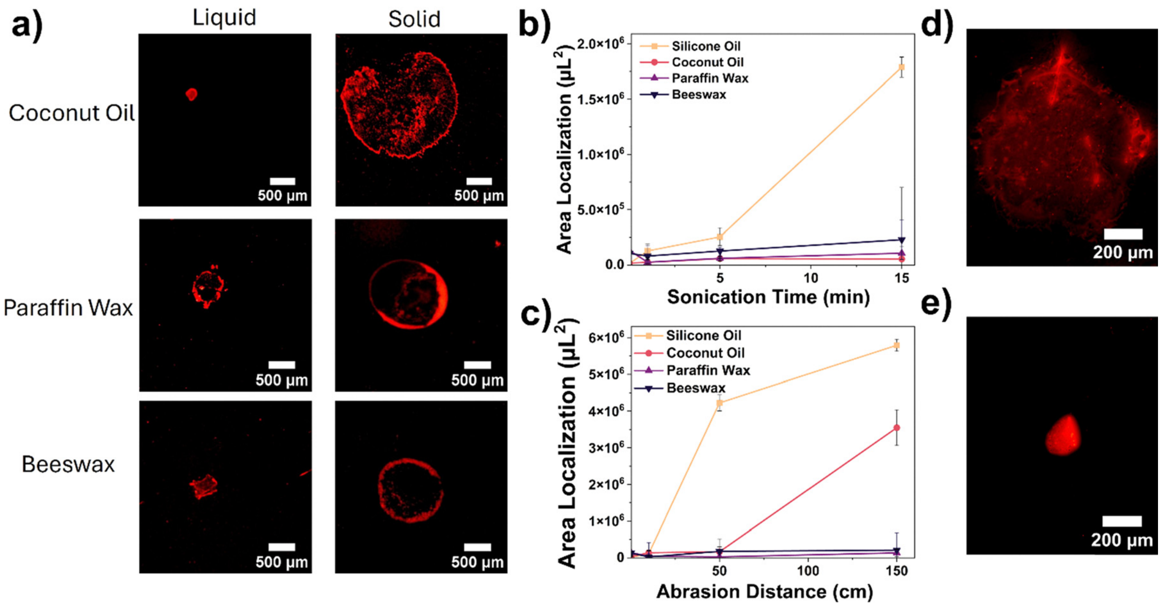

Fig. 5 Microplastic deposition and durability of PC-LIS under mechanical stress. (a) Fluorescent images of microplastic-laden droplets after evaporation on PC-LIS in liquid and solid states. (b) Quantified surface area of deposited analyte after repeated sonication (top) and (c) abrasion (bottom). Real microplastics from bottled water evaporated on (d) solid phase coconut oil surface and on (e) liquid phase coconut oil surface.

solid-phase PC-LIS becomes pinned, yielding larger and more diffuse deposition patterns, in line with past investigations.[94] We also quantified deposition areas on flat fluorosilane-coated silicon and on untreated nanograss substrates to see the effect of lubricant infusion and phase change. This showed localization values several orders of magnitude larger than PC-LIS and LIS surfaces, confirming that the underlying texture alone cannot account for the observed deposition areas, as shown in Table S3.

Fluorescent imaging of evaporated microplastic-laden droplets revealed distinct deposition patterns depending on the phase of the infused oil. Quantitative sensing performance was evaluated by extracting signal-to-noise (SNR) ratios across serial dilutions (0.01 to 0.000001%) and a detection limit (LOD) of 6×10^{-5}% was found, as shown in Table S4. Silicone oil, which does not exhibit phase transitions and maintains a consistent liquid interface, retained a small deposition footprint under both heated and cooled conditions, reflecting its stable low-pinning surface. In contrast, PC-LIS infused with coconut oil, paraffin wax, and beeswax showed a clear difference between liquid and solid phases. In the liquid state, evaporated drops on all three oils produced compact deposition spots due to enhanced droplet mobility and minimal contact line pinning promoting inward flow during evaporation. However, in the solid state, drops evaporated on these same oils yielded significantly larger and more diffuse deposition areas resulting from strong pinning and suppressed internal droplet flow.[95] To characterize particle transport during evaporation, we estimated the Peclet number ($\mathrm{Pe} = UR/D$), where U is the contact line velocity, R is the characteristic radius, and D is the particle diffusivity (estimated to 4×10^{-13} m^2 s^{-1} based on 1 μm microspheres). Since $\mathrm{Pe} > 1000$, advective flow dominates over diffusion, explaining the strong localization of particles and the sensitivity of deposition patterns to interfacial wetting conditions.[96] These observations confirm that switchable wettability in PC-LIS enables thermal control over analyte deposition geometry, offering a tunable platform for surface-based concentration and localization. Deposition experiments showed a several-orders-of-magnitude reduction in analyte localization size on PC-LIS compared to non-infused textured substrates, 1×10^5 μm^2 to 4.7×10^7 μm^2, respectively. The particle size distribution of the polystyrene microplastics was measured using a LiteSizer 500 (Anton Paar), yielding an average diameter of 1.08 μm (Fig. S6). Using this mean diameter and the droplet volume fraction (0.01%), the total number of particles in each droplet was estimated from the standard hard-sphere volume fraction and was found to be $\sim 4 \times 10^5$ particles per droplet.[97]

In addition to the model microplastics, we also extracted stained microplastics from bottled water (as described in the methods) to investigate whether the results from the model polypropylene spheres align with results from real microplastics, which exhibit significant variations in both size and shape. Fig. 5d and e show deposits from these real microplastics deposited from evaporating drops on both the liquid and solid states of PC-LIS, and demonstrate that localization trends from model spherical particles hold true for the complex, real microplastics. While the present results are based on droplets in otherwise pure water (DI water for the model spheres, and purified bottled water for the real microplastics), samples extracted from the environment will contain higher concentrations of salts, organics, and colloids. All of these components can modify wetting and deposition behavior.[98] Future adaptations may require accounting for these additional complexities associated with water chemistry.[99]

This localization behavior can be important for surface-based microplastic sensing and environmental diagnostics. Smaller deposition footprints enhance detection resolution by concentrating signal intensity, making PC-LIS in the liquid state ideal for localized sensing platforms. However, lubricant depletion under harsh conditions or shearing flows limits versatility of traditional LIS. Thus, the ability to switch between phases can combine the structural durability of wax-infused materials with the deposit localization functionality of LIS. In addition, some analytical techniques such as scanning electron microscopy (SEM) and Raman are difficult to perform on liquid infused samples, as the lubricant layer can evaporate or lead to surface charging that reduces image quality. By reverting back to solid form prior to analysis, the materials will also become more compatible with gold-sputter coating required to reduce surface charging and improve image quality. Similarly, Raman spectroscopy which is typically used in microplastic analysis to determine polymer chemistry, requires focusing of the laser on the sample. Localized particles captured on the solid wax material will not be in danger of moving, while particles on the extremely mobile liquid-phase materials may drift slightly during analysis and reduce signal intensity.

The performance of LIS in real-world settings depends on their mechanical stability. Fig. 5b/c quantify the area localization change before and after mechanical challenges. Silicone oil begins to have an increase in area localization after only 5 minutes of sonication, indicative of oil removal and return of the underlying superhydrophobic nanograss surface. Coconut oil and beeswax in the solid state also have a slight increase after 15 minutes of underwater sonication. The biggest transitions occurred after 15 minutes of sonication, showing that solid-phase PC-LIS, in contrast to liquid silicone oil, retained most of their initial wetting characteristics due to the immobile nature of the infused wax.

Abrasion tests showed similar trends: PC-LIS exposed to rubbing while in the solid state exhibited less change in area localization compared to silicone oil in the liquid state, suggesting greater mechanical integrity. Coconut oil was more sensitive to abrasion compared to beeswax and paraffin wax, likely reflecting the softer state of coconut oil in the solid state. These tests confirm that solid-state storage of the lubricant enhances structural robustness, while re-melting restores functionality for an advantageous trade-off between resilience and reconfigurability. We also report the change in contact angle hysteresis during the durability tests, which is another metric reflecting the retention of lubricant functionality under mechanical stress (Fig. S7).

Conclusions

Phase change liquid infused surfaces (PC-LIS) provide a powerful and tunable platform for controlling droplet wetting, evaporation, and deposition behavior through simple thermal modulation. By leveraging the reversible solid–liquid transitions of infused oils such as coconut oil, paraffin wax, and beeswax, PC-LIS surfaces exhibit dynamic shifts in contact angle hysteresis, sliding angle, and surface roughness. These changes in wetting properties will directly influence the drop evaporation mode and final analyte distribution. A strong correlation was observed between CAH and evaporation regime: surfaces with high CAH favored constant contact radius (CCR) behavior with extended droplet lifetimes, while low CAH states promoted constant contact angle (CCA) evaporation and more localized deposition.

Our results using model microplastic spheres as well as real microplastics from bottled water demonstrate the potential for these materials to localize analytes in the liquid state before switching back to the solid state for further analysis. The ability of these materials to localize even complex particle shapes including fibers and flakes from real microplastics is vital, as particle aspect ratio is known to profoundly influence deposit localization on non-LIS surfaces.[100]

In real environmental waters, the presence of other dissolved and colloidal matter may complicate analysis conducted from evaporating drops. For example, salts and dissolved ions will precipitate into crystals during evaporation, potentially blocking the signal for microplastics. To address this, it may be possible to tune the timing of phase change during drop evaporation to enhance separation of different species, which will precipitate from evaporating contact lines at different times based on solute size, shape, and other features.[101,102] Electrophoresis has also been previously applied to evaporating drop analyte sensing for separation of polystyrene microparticles and biological cells.[101] Similar principles could be applied using PC-LIS, which would increase mobility of the different materials and could thereby increase the responsivity to the applied electric field for separation of even smaller materials.

The ability to switch between pinned and mobile droplet states offers a functional advantage for on-demand control over microplastic deposition and localization with potential applications in environmental sensing, diagnostics, or microanalysis.[103,104] Other applications include anti-fouling for high-shear environments such as pipe interiors, where shearing forces would typically deplete lubricant from LIS. Using PC-LIS, the lubricant can be stored in the solid state, with any foulants periodically dislodged by heating-induced phase transition to the liquid state. The solid state of PC-LIS enhances durability under mechanical stress, as we demonstrate through our tests on sonication and abrasion, by preserving the lubricant within the textures for long-term performance compared to traditional LIS materials. The choice of phase changing lubricant will depend on the desired applications, with coconut oil giving the fastest dynamic response to heating due to its very low melting temperature at ~26 °C, but also being the softest and most compliant material tested here. Prior work has developed a robust catalog of PC materials, including wax mixtures, waxes containing nanoparticles, and other advanced materials to further tune properties and expand the range of functionalities for these materials.[12,31] Such advanced PC materials could be utilized for fabrication of new classes of PC-LIS whose properties would likely differ from those of bulk PC materials due to the very thin lengthscales involved.

Conflicts of interest

There are no conflicts of interest to declare.

Data availability

All data generated or analyzed during this study are included in this published article and its supplementary information (SI) files. Supplementary information: please see the uploaded videos (e-component). See DOI: https://doi.org/10.1039/d5sm00979k.

Additional datasets are available from the corresponding author on reasonable request.

Acknowledgements

We would like to thank Rehan Kumar, Renad Rawas, and Ranim Rawas, who helped with the deep-reactive ion etching to create the black silicon used in this study. Funding provided by the University of Pennsylvania. This work was carried out in part at the Singh Center for Nanotechnology, which is supported by the NSF National Nanotechnology Coordinated Infrastructure Program under grant NNCI-2025608. Gregory Parisi also thanks the Center for Soft and Living Matter at the University of Pennsylvania, where he is a Postdoctoral Fellow.

References

1 D. Quéré, Non-sticking drops, *Rep. Prog. Phys.*, 2005, **68**(11), 2495–2532, DOI: 10.1088/0034-4885/68/11/R01.
2 T. S. Wong, *et al.*, Bioinspired self-repairing slippery surfaces with pressure-stable omniphobicity, *Nature*, 2011, **477**(7365), 443–447, DOI: 10.1038/nature10447.
3 J. D. Smith, *et al.*, Droplet mobility on lubricant-impregnated surfaces, *Soft Matter*, 2013, **9**(6), 1772–1780, DOI: 10.1039/c2sm27032c.
4 Y. A. Lee, *et al.*, Slippery, Water-Infused Membrane with Grooved Nanotrichomes for Lubricating-Induced Oil Repellency, *Adv. Sci.*, 2022, **9**, 2103950, DOI: 10.1002/advs.202103950.
5 J. Wang, *et al.*, Understanding the role of infusing lubricant composition in the interfacial interactions and properties of slippery surface, *J. Colloid Interface Sci.*, 2024, **659**, 289–298, DOI: 10.1016/j.jcis.2023.12.174.
6 P. Flores, S. A. McBride, J. M. Galazka, K. K. Varanasi and L. Zea, Biofilm formation of Pseudomonas aeruginosa in spaceflight is minimized on lubricant impregnated

surfaces, *NPJ Microgravity*, 2023, **9**, 66, DOI: 10.1038/s41526-023-00316-w.

7 S. A. McBride, S. Dash and K. K. Varanasi, Evaporative Crystallization in Drops on Superhydrophobic and Liquid-Impregnated Surfaces, *Langmuir*, 2018, **34**(41), 12350–12358, DOI: 10.1021/acs.langmuir.8b00049.

8 S. B. Subramanyam, G. Azimi and K. K. Varanasi, Designing Lubricant-Impregnated Textured Surfaces to Resist Scale Formation, *Adv. Mater. Interfaces*, 2014, **1**, 2, DOI: 10.1002/admi.201300068.

9 S. Anand, A. T. Paxson, R. Dhiman, J. D. Smith and K. K. Varanasi, Enhanced condensation on lubricant-impregnated nanotextured surfaces, *ACS Nano*, 2012, **6**(11), 10122–10129, DOI: 10.1021/nn303867y.

10 Y. Hu, *et al.*, Enhanced condensation on liquid-infused nanoporous surfaces by vibration-assisted droplet sweeping, *ACS Nano*, 2020, **14**(10), 13367–13379, DOI: 10.1021/acsnano.0c05223.

11 K. C. Park, *et al.*, Condensation on slippery asymmetric bumps, *Nature*, 2016, **531**(7592), 78–82, DOI: 10.1038/nature16956.

12 S. Yun, S. Lee and K. Yong, Photo-responsive liquid–solid triboelectric nanogenerator by photothermal effect, *Nano Energy*, 2024, **129**, 110075, DOI: 10.1016/j.nanoen.2024.110075.

13 H. A. Stone, Ice-phobic surfaces that are wet, *ACS Nano*, 2012, DOI: 10.1021/nn303372q.

14 Z. Hao and W. Li, A review of smart lubricant-infused surfaces for droplet manipulation, *Nanomaterials*, 2021, DOI: 10.3390/nano11030801.

15 W. Yao, L. Wu, L. Sun, B. Jiang and F. Pan, *Recent developments in slippery liquid-infused porous surface*, Elsevier B. V., 2022, DOI: 10.1016/j.porgcoat.2022.106806.

16 X. Chen, G. Wen and Z. Guo, What are the design principles, from the choice of lubricants and structures to the preparation method, for a stable slippery lubricant-infused porous surface?, *Mater. Horiz.*, 2020, **7**(7), 1697–1726, DOI: 10.1039/d0mh00088d.

17 S. K. Laney, *et al.*, Delayed Lubricant Depletion of Slippery Liquid Infused Porous Surfaces Using Precision Nanostructures, *Langmuir*, 2021, **37**(33), 10071–10078, DOI: 10.1021/acs.langmuir.1c01310.

18 L. Mazor, H. A. Stone and I. Jacobi, Effect of streamwise cross-sectional variation on liquid retention in liquid-infused substrates under an external flow, *Phys. Rev. Fluids*, 2019, **4**, 074003, DOI: 10.1103/PhysRevFluids.4.074003.

19 S. Peppou-Chapman, J. K. Hong, A. Waterhouse and C. Neto, *Life and death of liquid-infused surfaces: A review on the choice, analysis and fate of the infused liquid layer*, Royal Society of Chemistry, 2020, DOI: 10.1039/d0cs00036a.

20 X. Lou, Y. Huang, X. Yang, H. Zhu, L. Heng and F. Xia, *External Stimuli Responsive Liquid-Infused Surfaces Switching between Slippery and Nonslippery States: Fabrications and Applications*, Wiley-VCH Verlag, 2020, DOI: 10.1002/adfm.201901130.

21 C. Chen, *et al.*, In Situ Electric-Induced Switchable Transparency and Wettability on Laser-Ablated Bioinspired Paraffin-Impregnated Slippery Surfaces, *Adv. Sci.*, 2021, **8**, 2100701, DOI: 10.1002/advs.202100701.

22 C. G. Jothi Prakash and R. Prasanth, *Approaches to design a surface with tunable wettability: a review on surface properties*, 2021, Springer, DOI: 10.1007/s10853-020-05116-1.

23 C. Li, M. Li, Z. Ni, Q. Guan, B. R. K. Blackman and E. Saiz, Stimuli-responsive surfaces for switchable wettability and adhesion, *J. R. Soc., Interface*, 2021, **18**, 20210162, DOI: 10.1098/rsif.2021.0162.

24 G. Parisi, X. Wang, Y. Hwang and S. Narayan, Assessing the Performance of a Thermoresponsive Liquid-Based Smart Windows for Building Thermal Regulation through Outdoor Experimentation and Computational Modeling, *Adv. Sustainable Syst.*, 2024, **8**, 2400237, DOI: 10.1002/adsu.202400237.

25 Y. Ru, R. Fang, Z. Gu, L. Jiang and M. Liu, Reversibly Thermosecreting Organogels with Switchable Lubrication and Anti-Icing Performance, *Angew. Chem., Int. Ed.*, 2020, **59**(29), 11876–11880, DOI: 10.1002/anie.202004122.

26 G. Parisi, A. Lopez and S. Narayan, A Dynamically Responsive Surface with Switchable Wettability for Efficient Evaporation and Self-Cleaning Abilities, *ACS Appl. Eng. Mater.*, 2023, **1**(1), 408–416, DOI: 10.1021/acsaenm.2c00097.

27 C. Qu, Y. Li, G. Li, X. Wang, M. Su and H. Liu, Liquid Interfacial Gating of Superhydrophobic Plasmonic Metal-Organic Frameworks for Three-in-One Separation, Enrichment, and Recognition in Bacterial Quorum Sensing, *ACS Appl. Mater. Interfaces*, 2024, **16**(25), 32824–32835, DOI: 10.1021/acsami.4c03661.

28 H. Zhu, W. Tu, X. Zhu, Y. Zhou and Z. Zou, Three-dimensional nanosheet glass with fluid-induced switchable haze obtained by hydrothermal method, *J. Non Cryst. Solids*, 2025, **650**, 123384, DOI: 10.1016/j.jnoncrysol.2024.123384.

29 G. Parisi and S. Narayan, A fluorine-free customizable membrane using sintered copper for oil/water and surfactant-stabilized water-in-oil emulsion separation, *Chem. Eng. Process.*, 2022, **181**, 109165, DOI: 10.1016/j.cep.2022.109165.

30 G. Parisi, P. K. Szewczyk, S. Narayan and U. Stachewicz, Thermoresponsive nanofiber yarns for water harvesting enhanced by harp system, *Chem. Eng. J.*, 2024, **499**, 155874, DOI: 10.1016/j.cej.2024.155874.

31 R. Chatterjee, U. Chaudhari and S. Anand, How to Select Phase Change Materials for Tuning Condensation and Frosting?, *Adv. Funct. Mater.*, 2023, **33**, 2206301, DOI: 10.1002/adfm.202206301.

32 Z. Zhang, Z. Chu, X. Liu, L. Fu, Y. Lv and X. Fan, Superhydrophobic surface with switchable wettability and self-monitoring for droplet transportation, *Surf. Interfaces*, 2024, **51**, 104547, DOI: 10.1016/j.surfin.2024.104547.

33 G. Parisi, P. K. Szewczyk, S. Narayan and U. Stachewicz, Photoresponsive Electrospun Fiber Meshes with Switchable Wettability for Effective Fog Water Harvesting in

Variable Humidity Conditions, *ACS Appl. Mater. Interfaces*, 2023, **15**(33), 40001–40010, DOI: 10.1021/acsami.3c07044.

34 Y. Song, *et al.*, Flexible Tri-switchable Wettability Surface for Versatile Droplet Manipulations, *ACS Appl. Mater. Interfaces*, 2022, **14**(32), 37248–37256, DOI: 10.1021/acsami.2c12890.

35 H. Jiang, *et al.*, NIR-Driven Self-Healing Phase-Change Solid Slippery Surface with Stability and Promising Anti-fouling and Anticorrosion Properties, *ACS Appl. Mater. Interfaces*, 2024, **16**(26), 34089–34099, DOI: 10.1021/acsami.4c05341.

36 M. Ye, *et al.*, Temperature-driven sustainable anti-scaling on phase-change lubricant-infused surface, *Sci. China Mater.*, 2024, **67**(8), 2515–2522, DOI: 10.1007/s40843-024-2895-4.

37 R. Chatterjee, D. Beysens and S. Anand, Delaying Ice and Frost Formation Using Phase-Switching Liquids, *Adv. Mater.*, 2019, **31**, 17, DOI: 10.1002/adma.201807812.

38 F. Wang, W. Ding, J. He and Z. Zhang, Phase transition enabled durable anti-icing surfaces and its DIY design, *Chem. Eng. J.*, 2019, **360**, 243–249, DOI: 10.1016/j.cej.2018.11.224.

39 X. Meng, Z. Wang, L. Wang, L. Heng and L. Jiang, A stable solid slippery surface with thermally assisted self-healing ability, *J. Mater. Chem. A*, 2018, **6**(34), 16355–16360, DOI: 10.1039/c8ta05886e.

40 S. Dash and S. V. Garimella, Droplet evaporation dynamics on a superhydrophobic surface with negligible hysteresis, *Langmuir*, 2013, **29**(34), 10785–10795, DOI: 10.1021/la402784c.

41 J. H. Guan, *et al.*, Evaporation of Sessile Droplets on Slippery Liquid-Infused Porous Surfaces (SLIPS), *Langmuir*, 2015, **31**(43), 11781–11789, DOI: 10.1021/acs.langmuir.5b03240.

42 D. Brutin and V. Starov, *Recent advances in droplet wetting and evaporation*, Royal Society of Chemistry, 2018, DOI: 10.1039/c6cs00902f.

43 S. Y. Misyura, V. S. Morozov, E. G. Orlova and V. A. Andryushchenko, Wetting, droplet evaporation and corrosion behavior of various composite and textured materials, *Ceram. Int.*, 2024, **50**(11), 19269–19282, DOI: 10.1016/j.ceramint.2024.03.026.

44 A. A. Günay, M. K. Kim, X. Yan, N. Miljkovic and S. Sett, Droplet evaporation dynamics on microstructured biphilic, hydrophobic, and smooth surfaces, *Exp. Fluids*, 2021, **62**, 153, DOI: 10.1007/s00348-021-03242-3.

45 D. H. Chang, F. Wang, S. P. Palecek and D. M. Lynn, Slippery Liquid-Infused Porous Surfaces Infused with Thermotropic Liquid Crystals Enable Droplet-Based, Naked-Eye Reporting of Changes in Peptide Structure and Protease Activity, *ACS Appl. Mater. Interfaces*, 2025, **17**(19), 27882–27894, DOI: 10.1021/acsami.5c02541.

46 C. Mu, *et al.*, Development of surface droplet evaporation-based sensing platform for screening lipase inhibitors, *Microchem. J.*, 2024, **205**, 111256, DOI: 10.1016/j.microc.2024.111256.

47 Y. Qu, *et al.*, Sugar detection using drop evaporation, *Droplet*, 2025, **4**, e150, DOI: 10.1002/dro2.150.

48 S. Yang, X. Dai, B. B. Stogin and T. S. Wong, Ultrasensitive surface-enhanced Raman scattering detection in common fluids, *Proc. Natl. Acad. Sci. U. S. A.*, 2016, **113**(2), 268–273, DOI: 10.1073/pnas.1518980113.

49 J. Li, H. Liu and J. Paul Chen, *Microplastics in freshwater systems: A review on occurrence, environmental effects, and methods for microplastics detection*, Elsevier Ltd, 2018, DOI: 10.1016/j.watres.2017.12.056.

50 L. Xie, K. Gong, Y. Liu and L. Zhang, *Strategies and Challenges of Identifying Nanoplastics in Environment by Surface-Enhanced Raman Spectroscopy*, American Chemical Society, 2023, DOI: 10.1021/acs.est.2c07416.

51 W. J. Shim, S. H. Hong and S. E. Eo, *Identification methods in microplastic analysis: A review*, Royal Society of Chemistry, 2017, DOI: 10.1039/c6ay02558g.

52 Z. Yu, *et al.*, Microplastic detection and remediation through efficient interfacial solar evaporation for immaculate water production, *Nat. Commun.*, 2024, **15**, 6081, DOI: 10.1038/s41467-024-50421-x.

53 A. Al Harraq, P. J. Brahana and B. Bharti, *Colloid and Interface Science for Understanding Microplastics and Developing Remediation Strategies*, American Chemical Society, 2025, DOI: 10.1021/acs.langmuir.4c03856.

54 X. Shi, *et al.*, Capturing, enriching and detecting nanoplastics in water based on optical manipulation, surface-enhanced Raman scattering and microfluidics, *Nature Water*, 2025, **3**(4), 449–460, DOI: 10.1038/s44221-025-00417-8.

55 M. Ebrahimi, S. Azizian, M. Eslamipanah and B. Jaleh, A Straightforward Approach for the Removal of Microplastics from Water: Utilization of SLIPS, *ACS Appl. Mater. Interfaces*, 2025, **17**, 41282–41291, DOI: 10.1021/acsami.5c07177.

56 T. H. Her, R. J. Finlay, C. Wu, S. Deliwala and E. Mazur, Microstructuring of silicon with femtosecond laser pulses, *Appl. Phys. Lett.*, 1998, **73**(12), 1673–1675, DOI: 10.1063/1.122241.

57 S. A. Mcbride, H.-L. Girard and K. K. Varanasi, Crystal critters: Self-ejection of crystals from heated, superhydrophobic surfaces, 2021. https://www.science.org.

58 M. Casey, F. Dano, T. Busch, D. G. K. Aboud and A. M. Kietzig, Investigating the Effects of Lubricant Infusion Methods on Polymer SLIPS, *ACS Appl. Mater. Interfaces*, 2024, **16**(28), 37328–37337, DOI: 10.1021/acsami.4c09014.

59 S. J. Goodband, S. Armstrong, H. Kusumaatmaja and K. Voltchovsky, Effect of Ageing on the Structure and Properties of Model Liquid-Infused Surfaces, *Langmuir*, 2020, **36**(13), 3461–3470, DOI: 10.1021/acs.langmuir.0c00059.

60 F. W. Wang, J. Sun and A. Tuteja, *Material Design for Durable Lubricant-Infused Surfaces That Can Reduce Liquid and Solid Fouling*, American Chemical Society, 2025, DOI: 10.1021/acsnano.5c03214.

61 L. K. Malla, R. Bhardwaj and A. Neild, Analysis of Profile and Morphology of Colloidal Deposits obtained from Evaporating Sessile Droplets, 2019.

62 D. Ho and J. Masura, Dyeing to Know: Harmonizing Nile Red Staining Protocols for Microplastic Identification, *Colorants*, 2025, **4**(2), 20, DOI: 10.3390/colorants4020020.

63 S. A. Mason, V. G. Welch and J. Neratko, Synthetic Polymer Contamination in Bottled Water, *Front. Chem.*, 2018, **6**, 407, DOI: 10.3389/fchem.2018.00407.

64 A. U. Rahman, S. M. Kabeb and F. H. Zulfkifli, *Functional hydrophobic coatings: Insight into mechanisms and industrial applications*, Elsevier B. V. 2025, DOI: 10.1016/j.porgcoat.2025.109187.

65 R. Gulfam and Y. Chen, Recent Growth of Wettability Gradient Surfaces: A Review, *Research*, 2022, **2022**, 9873075, DOI: 10.34133/2022/9873075.

66 T. Young, III. An essay on the cohesion of fluids, *Philos. Trans. R. Soc. London*, 1805, **95**, 65–87, DOI: 10.1098/rstl.1805.0005.

67 R. N. Wenzel, Resistance of solid surfaces to wetting by water, *Ind. Eng. Chem.*, 1936, **28**(8), 988–994, DOI: 10.1021/ie50320a024.

68 A. B. D. Cassie and S. Baxter, Wettability of porous surfaces, *Trans. Faraday Soc.*, 1944, **40**, 546, DOI: 10.1039/tf9444000546.

69 R. Üçüncüoğlu and H. Y. Erbil, Water Drop Evaporation on Slippery Liquid-Infused Porous Surfaces (SLIPS): Effect of Lubricant Thickness, Viscosity, Ridge Height, and Pattern Geometry, *Langmuir*, 2023, **39**(18), 6514–6528, DOI: 10.1021/acs.langmuir.3c00471.

70 G. McHale, R. Ledesma-Aguilar and G. G. Wells, Interfacial Strategies for Smart Slippery Surfaces, *J. Bionic. Eng.*, 2020, **17**(4), 633–643, DOI: 10.1007/s42235-020-0057-9.

71 S. P. Jesumathy, M. Udayakumar and S. Suresh, Heat transfer characteristics in latent heat storage system using paraffin wax, *J. Mech. Sci. Technol.*, 2012, **26**(3), 959–965, DOI: 10.1007/s12206-011-1017-4.

72 M. Mahlouji Taheri, S. A. Kia and A. Moosavi, Slippery mush-infused surfaces with effective and durable anti-icing and water harvesting performance, *J. Mater. Chem. A*, 2025, **13**(34), 28172–28188, DOI: 10.1039/D5TA03332B.

73 R. Seemann, *et al.*, Wetting morphologies and their transitions in grooved substrates, *J. Phys.: Condens. Matter*, 2011, **23**, 18, DOI: 10.1088/0953-8984/23/18/184108.

74 M. Villegas, Y. Zhang, N. Abu Jarad, L. Soleymani and T. F. Didar, Liquid-Infused Surfaces: A Review of Theory, Design, and Applications, *ACS Nano*, 2019, **13**(8), 8517–8536, DOI: 10.1021/acsnano.9b04129.

75 O. Myronyuk, E. Vanagas, A. M. Rodin and M. Wesolowski, Estimation of the Structure of Hydrophobic Surfaces Using the Cassie–Baxter Equation, *Materials*, 2024, **17**, 4322, DOI: 10.3390/ma17174322.

76 M. Villegas, Y. Zhang, N. Abu Jarad, L. Soleymani and T. F. Didar, Liquid-Infused Surfaces: A Review of Theory, Design, and Applications, *ACS Nano*, 2019, **13**(8), 8517–8536, DOI: 10.1021/acsnano.9b04129.

77 V. Edachery and R. Shashank, Influence of surface texture directionality and roughness on wettability, sliding angle, contact angle hysteresis, and lubricant entrapment capability, *Tribol Int*, 2021, **158**, 106932, DOI: 10.1016/j.triboint.2021.106932.

78 C. Zhang, *et al.*, Relationship between Viscosity and Resistance of Oil Film: A New Way to Investigate the Controllable Friction between Charged Interfaces Lubricated by Ionic Lubricating Oil, *Adv. Mater. Interfaces*, 2022, **9**, 2200229, DOI: 10.1002/admi.202200229.

79 H. H. Tran, D. Lee and D. Riassetto, *Wetting ridges on slippery liquid-infused porous surfaces*, Institute of Physics, 2023, DOI: 10.1088/1361-6633/acc87a.

80 C. Tangsathitkulchai, Y. Sittichaitaweekul and M. Tangsathitkulchai, Temperature effect on the viscosities of palm oil and coconut oil blended with diesel oil, *J. Am. Oil Chem. Soc.*, 2004, **81**(4), 401–405, DOI: 10.1007/s11746-004-0913-8.

81 V. Mishra, S. P. Singh, M. Singh, V. S. Chandel and R. Manohar, Optical, rheological, and dielectric properties of coconut oil between 100 kHz and 30 MHz, *Heliyon*, 2024, **10**, e34565, DOI: 10.1016/j.heliyon.2024.e34565.

82 G. Ferrer, *et al.*, Empirical equation to estimate viscosity of paraffin, *J. Energy Storage*, 2017, **11**, 154–161, DOI: 10.1016/j.est.2017.03.002.

83 J. Lim, H. S. Hwang and S. Lee, Oil-structuring characterization of natural waxes in canola oil oleogels: rheological, thermal, and oxidative properties, *Appl. Biol. Chem.*, 2017, **60**(1), 17–22, DOI: 10.1007/s13765-016-0243-y.

84 A. Bucio, R. Moreno-tovar, L. Bucio, J. Espinosa-dávila and F. Anguebes-franceschi, Characterization of beeswax, candelilla wax and paraffin wax for coating cheeses, *Coatings*, 2021, **11**(3), 1–18, DOI: 10.3390/coatings11030261.

85 R. Gulfam, T. En Huang, C. Lv, D. Orejon and P. Zhang, Condensation heat transfer on phase change slippery liquid-infused porous surfaces, *Int. J. Heat Mass Transfer*, 2022, **185**, 122384, DOI: 10.1016/j.ijheatmasstransfer.2021.122384.

86 V. Kumar, M. Kumawat, A. Srivastava and S. Karagadde, Mechanism of flow reversal during solidification of an anomalous liquid, *Phys. Fluids*, 2017, **29**, 12, DOI: 10.1063/1.5005139.

87 V. Kumar and S. Dash, Patterns during Evaporative Crystallization of a Saline Droplet, *Langmuir*, 2022, **38**(22), 10265–10273, DOI: 10.1021/acs.langmuir.2c01535.

88 S. A. McBride, S. Atis, A. A. Pahlavan and K. K. Varanasi, Crystal Patterning from Aqueous Solutions via Solutal Instabilities, *ACS Appl. Mater. Interfaces*, 2024, **16**(15), 70980–70990, DOI: 10.1021/acsami.4c12466.

89 S. Armstrong, G. McHale, R. Ledesma-Aguilar and G. G. Wells, Evaporation and electrowetting of sessile droplets on slippery liquid-like surfaces and slippery liquid-infused porous surfaces (SLIPS), *Langmuir*, 2020, **36**(38), 11332–11340, DOI: 10.1021/acs.langmuir.0c02020.

90 Y. C. Chuang, C. K. Chu, S. Y. Lin and L. J. Chen, Evaporation of water droplets on soft patterned surfaces, *Soft Matter*, 2014, **10**(19), 3394–3403, DOI: 10.1039/c3sm52719k.

91 H. Hu and R. G. Larson, Evaporation of a sessile droplet on a substrate, *J. Phys. Chem. B*, 2002, **106**(6), 1334–1344, DOI: 10.1021/jp0118322.

92 V. Charitatos, T. Pham and S. Kumar, Droplet evaporation on inclined substrates, *Phys. Rev. Fluids*, 2021, **6**, 084001, DOI: 10.1103/PhysRevFluids.6.084001.

93 H. Hu and R. G. Larson, Analysis of the effects of marangoni stresses on the microflow in an evaporating sessile droplet, *Langmuir*, 2005, **21**(9), 3972–3980, DOI: 10.1021/la0475270.

94 M. R. Gunjan and R. Raj, Dynamic Roughness Ratio-Based Framework for Modeling Mixed Mode of Droplet Evaporation, *Langmuir*, 2017, **33**(28), 7191–7201, DOI: 10.1021/acs.langmuir.7b01653.

95 R. D. Deegan, O. Bakajin, T. F. Dupont, G. Huber, S. R. Nagel and T. A. Witten, *Contact line deposits in an evaporating drop*.

96 W. D. Baines and D. F. James, *Evaporation of a Droplet on a Surface*, 1994. https://pubs.acs.org/sharingguidelines.

97 W. C. K. Poon, E. R. Weeks and C. P. Royall, On measuring colloidal volume fractions, *Soft Matter*, 2012, DOI: 10.1039/c1sm06083j.

98 D. Orejon, K. Sefiane and M. E. R. Shanahan, Stick-slip of evaporating droplets: Substrate hydrophobicity and nanoparticle concentration, *Langmuir*, 2011, **27**(21), 12834–12843, DOI: 10.1021/la2026736.

99 R. D. Deegan, O. Bakajin, T. F. Dupont, G. Huber, S. R. Nagel and T. A. Witten, Capillary Flow as the Cause of Ring Stains from Dried Liquid Drops, *Nature*, 1997, **389**, 827–829.

100 P. J. Yunker, M. A. Lohr, T. Still, A. Borodin, D. J. Durian and A. G. Yodh, Effects of particle shape on growth dynamics at edges of evaporating drops of colloidal suspensions, *Phys. Rev. Lett.*, 2013, **110**, 3, DOI: 10.1103/PhysRevLett.110.035501.

101 N. R. Devlin, K. Loehr and M. T. Harris, The separation of two different sized particles in an evaporating droplet, *AIChE J.*, 2015, **61**(10), 3547–3556, DOI: 10.1002/aic.14977.

102 T. S. Wong, T. H. Chen, X. Shen and C. M. Ho, Nanochromatography driven by the coffee ring effect, *Anal. Chem.*, 2011, **83**(6), 1871–1873, DOI: 10.1021/ac102963x.

103 S. R. Karunathilaka, B. J. Yakes, K. He, L. Brückner and M. M. Mossoba, First use of handheld Raman spectroscopic devices and on-board chemometric analysis for the detection of milk powder adulteration, *Food Control*, 2018, **92**, 137–146, DOI: 10.1016/j.foodcont.2018.04.046.

104 E. Battaglini, P. Miralles, N. Lotti, M. Soccio, M. Fiorini and C. Coscollà, Analysis of microplastics in commercial vegetable edible oils from Italy and Spain, *Food Chem.*, 2024, **443**, 138567, DOI: 10.1016/j.foodchem.2024.138567.